

Assessing the impact of ~~landwater~~riverine water on the Northwest Pacific using normalized Total Alkalinity

Tatsuki Tokoro^{1, 6}, Shin-Ichiro Nakaoka¹, Shintaro Takao¹, Shu Saito^{2, 3, 4}, Daisuke Sasano³, Kazutaka Enyo³, Masao Ishii⁴, Naohiro Kosugi⁴, Tsuneo Ono⁵, Kazuaki Tadokoro⁵, and Yukihiro Nojiri¹

¹formaly at: Earth System Division, National Institute for Environmental Studies, Tsukuba, Japan.

²Administration Department, Japan Meteorological Agency, Tokyo, Japan.

³Atmosphere and Ocean Department, Japan Meteorological Agency, Tokyo, Japan.

⁴Department of Climate and Geochemistry Research, Meteorological Research Institute, Tsukuba, Japan.

⁵Fisheries Resources Institute, Japan Fisheries Research and Education Agency, Yokohama/Shiogama, Japan.

⁶currently at: Seto Inland Carbon-Neutral Research Center, Hiroshima University, Hiroshima, Japan.

Corresponding author: Tatsuki Tokoro (tokorota@hiroshima-u.ac.jp, tokoro.tatsuki@nies.go.jp)

Formatted: Superscript

Abstract. The impact of ~~landwater~~riverine water was assessed using salinity-normalized Total Alkalinity observations. The observational data included surface carbonate parameters from decades of surveys conducted by volunteer cargo ships and research vessels in the Northwest Pacific. Statistical processes, such as re-gridding and Fourier regression, used in a previous study were also applied in this study to improve the spatiotemporal resolution. First, the seawater area affected by ~~landwater~~riverine water was identified using an Empirical Orthogonal Function analysis of normalized Total Alkalinity. The differences in normalized Total Alkalinity and Dissolved Inorganic Carbon from the surrounding area were then analysed to evaluate the causes such as ~~landwater~~riverine water supply, advection effects, and biological activities. In addition, the impact of ~~landwater~~riverine water on oceanic CO₂ uptake and acidification in the study area was assessed. The analysis showed that ~~landwater~~riverine water was the main source of total coastal Alkalinity but was not the dominant cause of Dissolved Inorganic Carbon. The supply of ~~landwater~~riverine water had little effect on oceanic CO₂ uptake throughout the year. The supply of by ~~landwater~~riverine water was a factor in coastal acidification; however, the supplied Total Alkalinity reduced the overall acidification trend by 65%. The results of this study are expected to be further improved by enhancing observations, such as the vertical profiles of carbonate parameters, and are expected to expand to other sea areas and be applied to global budgets.

1. Introduction

The flow of ~~landwater~~riverine water to the ocean is one of the most important flows in the Earth's system. In the carbon cycle, ~~landwater~~riverine water is the major carbon source for the oceans (Aufdenkampe et al., 2011; Bauer et al., 2013; Borges et al., 2005; Cai, 2011; Chen and Borges, 2009; Chen et al., 2013), which is responsible for atmospheric CO₂ emissions and acidification in coastal areas (Carstensen and Durate, 2019; Duarte et al., 2013; Tranvik et al., 2009). However, strong carbon flows, such as biological pumps, impact carbonate distribution in coastal areas (Passow and Carlson, 2012; Regnier et al., 2013, 2022). ~~For example, increased biological pump in coastal areas will increase CO₂ absorption from atmosphere, but it will also progress the anoxia on the sediment. In coastal areas, the decomposition of organic matter supplied by riverine water is expected to cause more severe acidification, which may cause harmful algal growth and adversely affect marine products such as bivalves (Fitzer et al., 2018; Kessouri et al., 2021; Wallace et al., 2014).~~ Quantifying these complex flows is important for predicting future climate change and ocean acidification as well as for predicting biochemical changes in coastal areas.

The Northwest Pacific Ocean, including the coastal areas of Japan, ~~plays a crucial role in global carbon cycle due to the strong is one of the strongest sinks of atmospheric CO₂ (Takahashi et al., 2002, 2009). Therefore, it is crucial to assess the impacts of landwater on oceanic CO₂ uptake and coastal acidification.~~

While several studies on carbonate systems have been conducted in the Northwest Pacific Ocean (e.g., Ishii et al., 2001; Murata et al., 1998; Takamura et al., 2010; Tokoro et al., 2023; Yoshikawa-Inoue et al., 1995, 2014), spatiotemporal variations in ~~landwater~~riverine water in seas~~contribution~~ in this region have not yet been quantified. ~~Landwater~~Riverine water tracers (e.g., salinity, stable isotope, geogenic solutes like silica) are one of the most effective methods for evaluating the influence of ~~landwater~~riverine water. Although salinity is the most frequently assessed factor in ~~land-water~~riverine water transportation, other factors such as precipitation and evaporation also impact ~~this transportation~~salinity. This ~~omission~~ can be ~~source~~source of major error in the assessment of ~~and~~-water transportation in the northwestern Pacific region, where high precipitation and evaporation by low-pressure systems and heat waves, respectively, have been observed (Kitamura et al., 2016; Miyama et al., 2021; Sugimoto et al., 2013).

The total Alkalinity (TA) normalized by salinity is a potential indicator to assess the influence of ~~landwater~~riverine water on ocean. TA is a carbonate parameter in seawater and is defined ~~broadly~~ by the charge ~~balance~~difference between the proton donor and acceptor of dissolved ions, such as hydrogen carbonate (see Zeebe and Wolf-Gladrow, 2001 for more detailed definition). TA ~~depends on~~changes by several factors, such as advection from different water masses and biological metabolism, including the calcification and dissolution of calcium carbonate (e.g., Broecker and Peng, 1982; Lee et al., 2006; Millero et al., 1998). ~~Because~~ TA is also highly correlated with salinity; ~~however~~, TA normalized to the reference salinity (nTA) has been used to quantify the above factors (e.g., Broecker and Peng, 1982; Lee et al., 2006; Millero et al., 1998). nTA is calculated as follows:

$$nTA = TA \cdot \frac{s_{ref}}{s} \quad (1)$$

Formatted: Subscript

Formatted: Font: (Asian) MS 明朝, (Asian) Japanese

where, S and S_{ref} are the measured and reference salinities (traditionally 35), respectively. Similarly, Dissolved Inorganic Carbon concentration (DIC) was also normalized (nDIC). Equation (1) is formulated based on the assumption that a water mass with zero salinity has zero TA, otherwise the right-hand side would go to infinity. However, this assumption is not true for landwater/riverine water because its TA is greater than zero, even when salinity is zero, owing to the weathering of carbonate and silicate rocks (e.g., Friis et al., 2003; Lehmann et al., 2023; Rassmann et al., 2016; Taguchi et al., 2009). Therefore, when Equation (1) is applied to areas affected by landwater/riverine water, the nTA value is higher than that of the surrounding seawater. Conversely, the influence of landwater/riverine water, along with factors such as water mass advection and biological metabolism, can be quantified by assessing the distribution of nTA. Unlike other methods that use salinity as a tracer for landwater/riverine water, nTA defined in Equation (1) excludes the effect of precipitation and evaporation, which is advantageous because contamination by water masses with almost zero salinity and TA can be excluded. It is also easier to quantify the influence of seawater from different local areas because the TA has different values in different local areas, even if the salinity is the same (Lee et al., 2006; Takatani et al., 2014).

In this study, we aimed to analyse the influence of landwater/riverine water on carbonate systems in the ocean using nTA and other carbonate parameters measured by voluntary cargo ships and research vessels in the Northwest Pacific. First, spatiotemporal variations in the area in which landwater/riverine water significantly affected surface seawater were identified using Empirical Orthogonal Function (EOF) analysis of the nTA distribution. Second, we focused on the differences in TA and DIC between the landwater/riverine water-affected area and surrounding areas, ~~and~~ We quantified the landwater/riverine water supply and other contributing factors that affect TA and DIC. The final step involved the evaluation of the effects of landwater/riverine water on the environment in riverine water-affected area. Seawater CO_2 fugacity ($f\text{CO}_2$) and the calcite saturation state of seawater (Ω_{cal}) were the two carbonate parameters that were used as the index of environmental changes caused by landwater/riverine water input. The former parameter affects ~~the~~ air-sea CO_2 flux. The TA and DIC supplied by landwater/riverine water should change seawater $f\text{CO}_2$ and oceanic CO_2 uptake. Meanwhile, Ω_{cal} is the ratio of the concentration product of $[\text{Ca}^{2+}]$ and $[\text{CO}_3^{2-}]$ to the solubility product of calcite and is an index of ocean acidification. Calcite is a mineral composed of CaCO_3 and constitutes foraminifera, coccolithophorids, and the outer layer of bivalves. In coastal areas, the decomposition of organic matter supplied by landwater is expected to cause more severe acidification, which may cause harmful algal growth and adversely affect marine products such as bivalves (Fitzer et al., 2018; Kessouri et al., 2021; Wallace et al., 2014). Therefore, the analysis of changing Ω_{cal} is expected to lead to a more detailed assessment of coastal acidification in the study area. This study also aimed to evaluate the effects of landwater/riverine water on future climate change and coastal acidification and to predict the effects of future environmental changes.

Formatted: Subscript

Formatted: Font: (Asian) MS 明朝, (Asian) Japanese

2. Methods

2.1 Data for analysis

The observational data in this study were collected by the National Institute for Environmental Studies (NIES), Meteorological Research Institute (MRI) of the Japan Meteorological Agency (JMA), and Japan Fisheries Research and Education Agency (FREA). The NIES data were produced as part of the Voluntary Observing Ship (VOS) programs for cargo ships (namely, M/S Alligator Hope, M/S Pyxis, M/S New Century 2, and M/S Trans Future 5). MRI, JMA, and FREA collected data from research vessels (R/V Mirai and R/V Hakuho-maru for MRI; R/V Keifu-maru and R/V Ryofu-maru for JMA; and R/V Wakataka-maru and R/V Soyo-maru for FREA). These data were uploaded to the Surface Ocean CO₂ Atlas (SOCAT; Pfeil et al., 2013; Bakker et al., 2016, <https://socat.info/index.php/data-access/>) and Global Ocean Data Analysis Project (GLODAP, Key et al., 2015; Olsen et al., 2016; Olsen et al., 2020, <https://glodap.info/>). These observations were statistically processed by re-gridding, a second-order approximation of TA, carbonate equilibrium calculations, and Fourier regression into datasets with a spatial resolution of $1^\circ \times 1^\circ$ and a temporal resolution of 0.1 year, as suggested in a previous study (Tokoro et al., 2023). Similar to the previous study, the data was excluded from the analysis if there was insufficient temporal data ($n \geq 60$, correspond to 6 years data) in the $1^\circ \times 1^\circ$ spatial grid. Although the time interval (from January 1, 2000, to December 31, 2019), covered area (latitudes of 20–50°N and longitudes of 120–160°E), and original observations in the SOCAT by NIES were the same as those in the previous study, the original observations by MRI and JMA increased slightly (287750 to 291138) with the upgrade of the product (SOCAT ver. 2019 to 2023). The FREA dataset is a new addition to those used in previous studies. As the FREA data ($n = 566175$) were collected every 1 minute while the other data were collected every 10 min, the FREA data were weighted 1/10 with respect to the other data and weighted averaged as the gridded data. The GLODAP data for surface (<10 m depth) TA and DIC from the MRI and JMA were updated using ver. 2.2020 to 2.2023. The number of data points for JMA data increased from 2080 to 2163. However, the effect of increase in the data was small, which did not statistically affect the result (Table S1). Additionally, observations up to a depth of 150 m within the GLODAP were used to evaluate the effects of vertical advection (Text S1).

2.2 EOF analysis, Cause Analysis, and Environmental Impact Assessment

In this study, areas significantly affected by landwater/riverine water were identified by applying EOF analysis to the spatiotemporal variability of nTA. The EOF analysis breaks down spatiotemporal variations into multiple orthogonal modes with multiple spatial patterns (principal EOF patterns) and time series (principal component time series) (e.g., Denbo and Allen, 1984). In addition to the effect of riverine water, the target area in this study is assumed to be subject to a mixture of multiple fluctuations, such as seasonal fluctuations of the Kuroshio and Oyashio flows. Compared to the direct use of carbonate parameters, the EOF analysis is expected to identify the influence of riverine water because the analysis is appropriate to quantify and separate multiple fluctuations. Using the principal EOF pattern and principal component time

series with respect to the spatiotemporal variation of nTA, we identified ~~the area that~~ “Area A” was significantly influenced by ~~landwater~~ riverine water and labelled as “Area A”. ~~W~~Thereafter, we ~~then~~ labelled the surrounding area ~~with almost the same area~~ as “Area B.” The influence of ~~landwater~~ riverine water was quantified as the value of Area A minus that of Area B (dAB) for all related parameters such as SST (Sea Surface Temperature), SSS (Sea Surface Salinity), nTA, and nDIC.

130 Causal analysis of dAB of TA and DIC was performed using the following equation:

$$\frac{\partial dAB}{\partial t} = Sup_{rw} + C_{flux} + C_{res} \quad (2)$$

The left-hand side of the equation represents the time derivative of dAB of nTA and nDIC, ~~calculated from the normalized values (nTA and nDIC, respectively) to exclude the effect of seawater volume change due to landwater inflow.~~ Sup_{rw} , Sup_{rw} is the TA or DIC supply by ~~landwater~~ riverine water; C_{flux} is the term of difference in air-sea CO_2 flux between Areas A and B divided by ~~mixed layer depth (-MLD), which~~ The MLD with the same spatiotemporal resolutions as the processed data ($1^\circ \times 1^\circ$ and 0.1 year) ~~is the mixed layer depth~~ was calculated from the reanalysis data of seawater temperature profiles by Japan Agency for Marine-Earth Science and Technology (JCOPE2M; Miyazawa et al., 2017, 2019, <https://www.jamstec.go.jp/jcope/htdocs/distribution/>). We determined an ~~as~~-isothermal depth at $\Delta T = 0.2^\circ C$ with linear interpolation (de Boyer Montégut et al., 2004; Holte and Talley, 2009); ~~this term~~ C_{flux} was applied only to the DIC input. C_{res} is the TA or DIC input due to other residual factors related to dAB (e.g., horizontal and vertical advection and biological metabolism).

Sup_{rw} , Sup_{rw} was estimated from river discharge and TA or DIC in river water as follows:

$$Sup_{rw} = \frac{Flow_r \cdot C_r}{MLD \cdot A} \quad (3)$$

where, $Flow_r$ is the monthly total flow rate of the river, C_r represents the TA or DIC of the associated rivers, A is the area of Area A. The flow rate was estimated using the Water Information System database of the Ministry of Land, Infrastructure, Transport, and Tourism of Japan (<http://www1.river.go.jp/>). As TA and DIC data were not available for all rivers, the referential values for zero-salinity endmembers in the three most river-influenced inner bays (Tokyo Bay, Ise Bay, and Osaka Bay) in the relevant coastal areas were used (518–1006 and 475–1371 $\mu mol\ kg^{-1}$ for TA and DIC, respectively; Taguchi et al., 2009; Tokoro et al., 2021). ~~The DIC range includes the value predicted as the range of seasonal variation ($\pm 200\ \mu mol\ kg^{-1}$, Tokoro et al., 2021). Notably, Although~~ TA range did not consider seasonal variations; ~~however,~~ the ~~range is effect estimated to be an order of magnitude smaller than the range of spatial differences among the three bays from the literature value (Romero-Mujalli et al., 2018) was more pronounced.~~ All data were regridded to the resolution of the processed SOCAT and GLODAP data (spatial and temporal resolution of $1^\circ \times 1^\circ$ and 0.1 year, respectively). Air-sea CO_2 flux (F) was determined as follows:

$$F = k \cdot K_0 \cdot (fCO_{2water} - fCO_{2air}) \quad (4)$$

where, k is transfer velocity defined by the wind speed above the sea surface (Wanninkhof, 2014). K_0 is the solubility of CO_2 in seawater and was calculated using an empirical equation based on SST and SSS (Weiss, 1974). fCO_{2water} and fCO_{2air} are the fCO_2 in surface seawater and air, respectively. C_{flux} was determined by the difference in air-sea

Formatted: Font: Not Italic

Formatted: Default Paragraph Font

Formatted: Font: Italic

Formatted: Font: Italic, Subscript

Formatted: Font: (Default) +Body (Times New Roman)

Formatted: Font: (Asian) MS 明朝, (Asian) Japanese

Formatted: Font: Italic

Formatted: Font: Italic

Formatted: Subscript

Formatted: Font: Italic

Formatted: Font: Italic, Subscript

~~fCO₂ flux difference~~ between Areas A and B, which was calculated from the processed fCO₂ data and wind velocity from the database of the Cross-Calibrated Multi-Platform (CCMP, Atlas et al., 2011; Mears et al., 2019, <https://data.remss.com/ccmp/v02.0/>, version 2.0). The details of the calculations are the same as those used in a previous study (Tokoro et al., 2023).

~~The effect of landwater/riverine water on air-sea CO₂ flux and acidification were quantified by multivariate analysis using *dAB* of seawater fCO₂ and Ω_{cal} as the objective variables and *dAB* of SST (Sea Surface Temperature), SSS (Sea Surface Salinity), nTA, and nDIC as the explanatory variables. Ω_{cal} was determined using the equation of a calcite solubility product (Mucci, 1983) and the concentration of Ca²⁺ and CO₃²⁻ estimated using the CO₂SYS program (Lewis and Wallace, 1998). Although both seawater fCO₂ and Ω_{cal} can be unambiguously determined from equilibrium calculation using SST, SSS, nTA, and nDIC (Zeebe and Wolf-Gladrow, 2001). However, it is difficult to intuitively understand the contribution of the explanatory variables, a multivariate linear model should be useful because these have a non-linear relationship, and it is difficult to intuitively understand the contribution of the explanatory variables. Therefore, we considered that a multivariate linear model should be useful in this study.~~ Partial least squares regression (PLS regression; Wold et al., 2001) was used in the multivariate analysis to prevent multicollinearity, especially considering the strong correlation between SSS and nTA and nDIC.

Formatted: Font: (Asian) MS 明朝, (Asian) Japanese

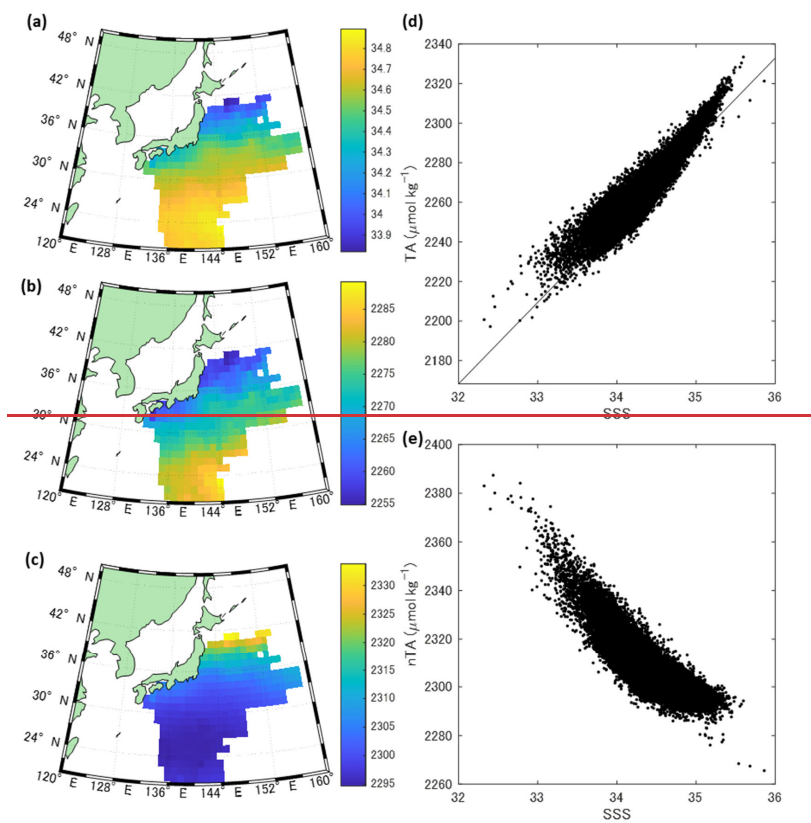
Formatted: Not Superscript/ Subscript

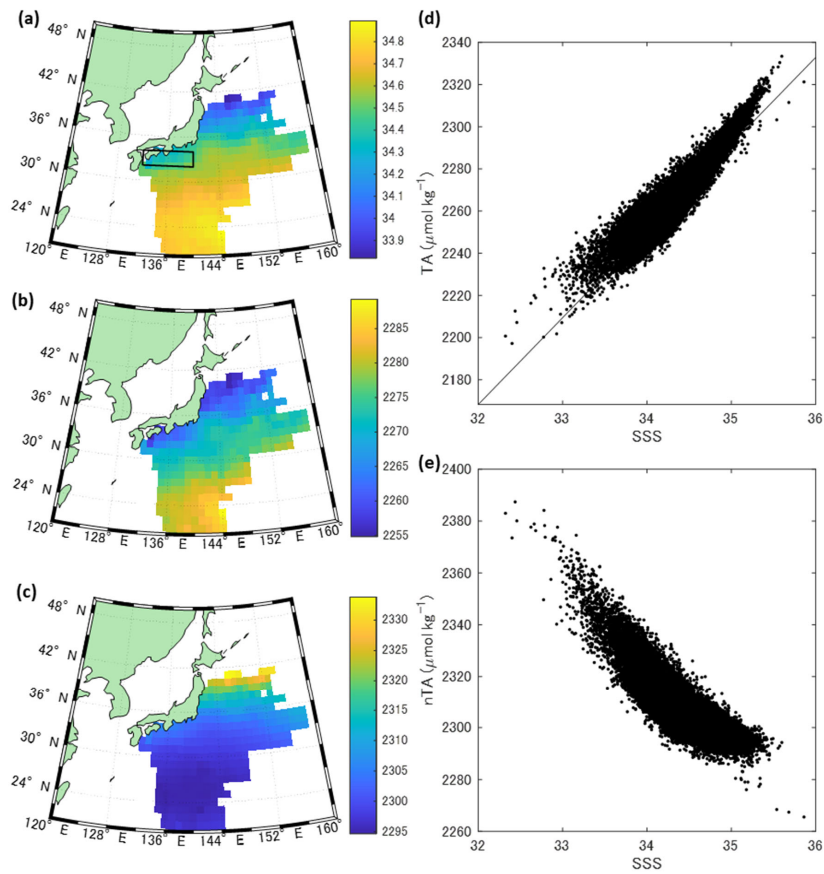
Formatted: Font: (Asian) MS 明朝, (Asian) Japanese, Not All caps

3. Results

Figure 1 represents the processed spatial distributions of SSS, TA, and nTA. The SSS showed a north-south gradient, which was attributed to ~~the high-salinity Kuroshio current and the relatively low salinity Oyashio current-freshwater inflow from the Amur River in the north and high evaporation at horse latitudes.~~ There was also an area of reduced SSS along the Pacific coast of mainland Japan (32–34°N, 132–140°E; Figure 1a). These trends were similar for TA, which exhibited high correlation with SSS ($R^2 = 0.94$) (Figure 1b, d). The nTA was high in the northern part of the study area, and slightly high values were also observed along the Pacific coast of Japan (Figure 1c). The intercept of the regression line between SSS and TA was $528.04 \pm 2.00 \mu\text{mol kg}^{-1}$ (Ave \pm SE), which was consistent with the TA value of ~~large river on the continental side like~~ the Amur River ($589 \mu\text{mol kg}^{-1}$; Andreev and Pavlova, 2009) and Japanese river water ($518\text{--}1006 \mu\text{mol kg}^{-1}$) (Figure 1d). ~~In contrast, because the intercept value was above zero, nTA seemed to be~~ inversely proportional to SSS ($R^2 = 0.57$), with a lower SSS tending to have a higher nTA (Figure 1e). These results indicate that the study area was affected by freshwater with TA above zero, especially in the northern area and on the Pacific coast of Japan, ~~and that nTA could be used as a tracer for the freshwater input.~~

Formatted: Font: (Asian) MS 明朝, (Asian) Japanese





190 **Figure 1 (a–c):** Spatial distribution of (a) mean SSS (b) TA and (c) nTA. The rectangular in (a) show the reduced SSS area along the Pacific coast of mainland Japan (32–34°N, 132–140°E) (d and e): Scatterplot of (d) SSS-TA and (e) SSS-nTA. The black line is the approximate line ($R^2 = 0.94$, $TA = (50.46 \pm 0.06) \times SSS + (528.04 \pm 2.00)$ (Ave. \pm SE)).

The spatial distribution of nTA in the three most dominant modes of the EOF analysis is shown in Figure 2(a–c). The principal EOF patterns were indicated by a parameter defined as “EOF anomaly,” denoted by red or blue in Figure 2. The spatiotemporal variation of the nTA anomaly in each mode was expressed as the product of the EOF anomaly and the principal component time series. In the most dominant mode (Mode 1), the principal patterns exhibited a clear north-south difference at approximately 37°N (Figure 2a). The principal component of the time series in Mode 1 (Figure 2d) indicated that the annual cycle was predominant, and an annual maximum of nTA was observed in summer and winter in the area south and north of 37°N, while it was in winter in the area north of 37°N respectively (data not shown). The seasonal variation south of 37°N can be explained by the fact that landwater riverine water supply is proportional to the precipitation over land, thereby reaching its peak in summer on the Pacific side of Japan (Database of Japan Meteorological Agency, <https://www.data.jma.go.jp/stats/etrn/index.php>). For the area north of 37°N, this may be due to the southward transportation of high-nTA surface seawater in the Pacific subarctic region by northerly winds in winter or winter vertical mixing that supplied subsurface high-nTA seawater to the surface. In addition, the EOF anomaly south of 37°N was significantly correlated with distance from the Japanese mainland (Figure 2e). Because EOF anomaly is a parameter indicating the strength of annual cycle fluctuation in nTA, as shown in Figure 2d, Figure 2e indicates that the degree of temporal variation in nTA increased significantly closer to mainland Japan in this mode. The degree of temporal variation in nTA, as shown in Figure 2d, increased significantly closer to mainland Japan in this mode. The other major modes (Modes 2 and 3; Figure 2b, c) had an east-west distribution north of 37°N. A distribution such as this could represent seasonal or multi-year variations in the flow path of the Kuroshio Extension. After mode 4, the variation north of 37°N was also explained, and thus mode 1 was dominant for the variation south of 37°N.

Based on the above considerations, we determined that it was appropriate to use the Mode 1 EOF anomaly south of 37°N as an indicator of the influence of landwater riverine water from mainland Japan. Although the area north of 37°N contains Japanese rivers with large flow rates (e.g., the Kitakami River), the effect of landwater riverine water was excluded from the analysis in this study because the influence of high nTA in the subarctic gyre was too dominant to extract the influence of landwater riverine water from Japan. The influence of subarctic Pacific seawater can be expected even around 37°N; however, this is not expected to have a significant effect on the statistics in Area A, such as the spatial mean values. Area A is located south of 37°N and within 246.6750 km of land (Figure 2f). This distance is defined using change-point detection (Killick et al., 2012), meaning that the mean EOF anomaly south of 37°N changes abruptly before and after this distance. The outer edge of Area A roughly aligned with the Kuroshio axis, as indicated by the JCOPE2 SSH data (SSH = 0.2 m). Although the EOF anomaly outside Area A also shows a relatively weak correlation with distance, this correlation is thought to be due to the influence of landwater riverine water from areas other than Japan, such as East Asia, which was difficult to quantify using the measurement data in this study. To minimize the influence of landwater riverine water outside Japan and differences in latitude and longitude, Area B was determined as adjacent to Area A, similar in size to the area for comparison (Figure 2f).

Formatted: Font: Century

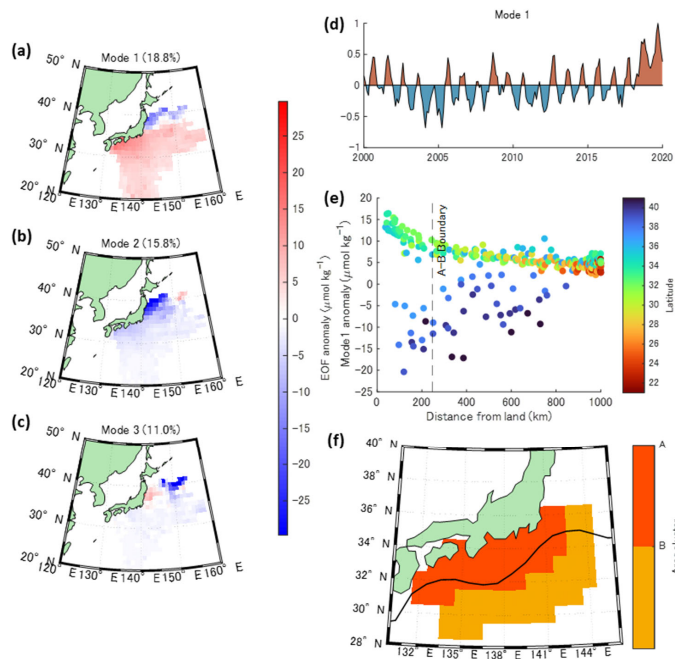
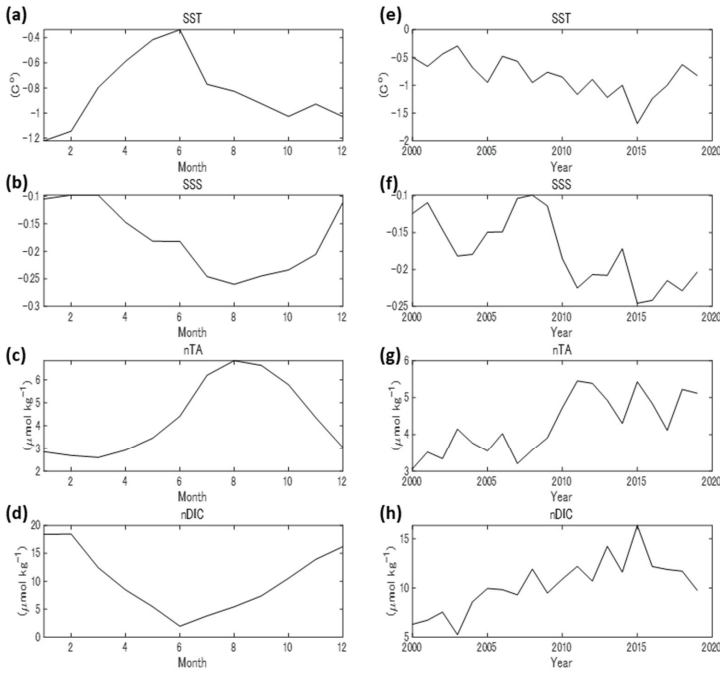


Figure 2. (a–c): EOF anomaly of (a) Mode 1, (b) Mode 2, and (c) Mode 3. The percentage in the bracket (18.8%) indicates the contribution of this mode to the original variation. (d): Principal component of time series of Mode 1. (e): Scatterplot of EOF anomaly of Mode 1 versus distance from Japan mainland. The plot colours indicate the latitude. The dotted line represents the boundary of Areas A and B estimated using the changepoint analysis. (f): Distribution of Area A and B. The black curve indicates mean Kuroshio axis during the whole period in this study (2000–2019).

—The monthly and annual average values of the differences in the relevant parameters (SST, SSS, nTA, and nDIC) between Areas A and B (dAB) are shown in Figure 3. All dAB parameters showed seasonal variation, and the absolute values of dAB were largest in winter for SST and nDIC and in summer for SSS and nTA. On a decadal scale, the absolute values of all dAB tended to increase significantly. This indicates an increase in the supply of riverine water, which is consistent with the Japan

240 Meteorological Agency's report (<https://www.data.jma.go.jp/cpd/cgi-bin/view/index.php>) that precipitation in relevant areas of Japan increased during the period analysed in this study.

—This indicates that the supply of landwater was on increase, and is consistent with the fact that precipitation in relevant areas in Japan was reported to have been increasing during the period analyzed in this study by the Japan Meteorological Agency (<https://www.data.jma.go.jp/cpd/cgi-bin/view/index.php>).



245 **Figure 3. The differences in SST, SSS, nTA, and nDIC between Areas A and B (*dAB*). (a)–(d): Seasonal variations. (e)–(h): Annual variations. Although the time step in this study was 0.1 year, the monthly values were calculated by spline interpolation of values at 1/12-year intervals. The same applies to the other figures.**

250 —Figure 4 represents the time-series variations of each term in Equation (2) used for the causal analysis of the *dAB* of nTA and nDIC. The river discharge for $Sup_{hr}-Sup_{rw}$ was calculated as the sum of the 37 rivers bordering Area A (see Text S2). The maximum nTA and nDIC $Sup_{hr}-Sup_{rw}$ were observed during the summer months, when precipitation on the Pacific coast

of Japan was the highest. Though the air-sea CO_2 flux term (C_{flux}) also showed a clear seasonal variation, the annual average did not. The residual term (C_{res}) tended to be negative for both TA and DIC; however, the seasonal patterns and ranges of variation differed considerably.

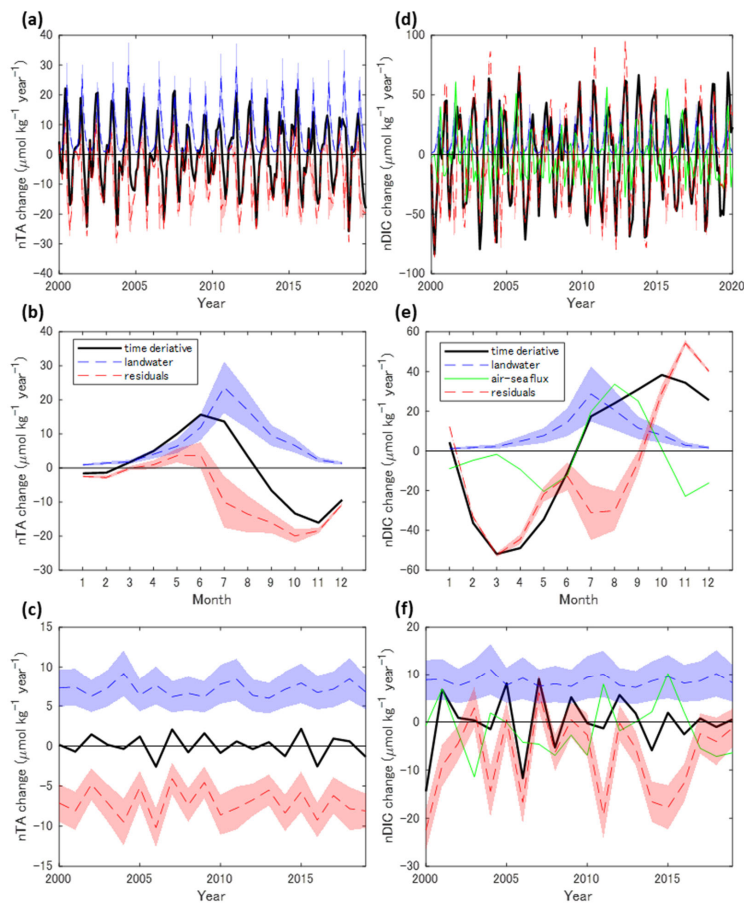
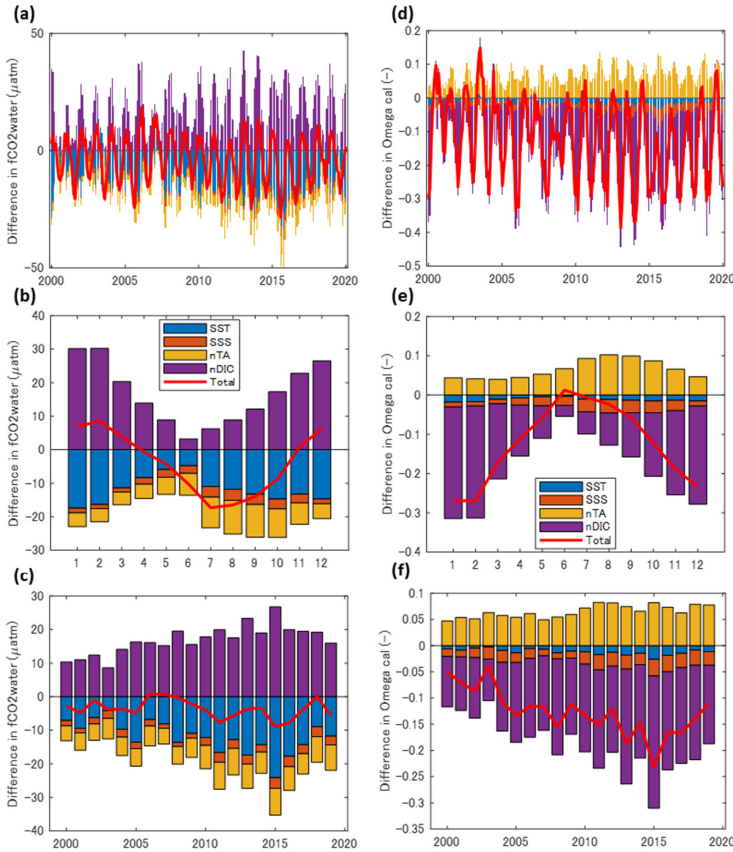


Figure 4. (a): Temporal variations of nTA time derivative and related terms in Equation (2). (b): The monthly averages. (c): The yearly averages. (d)-(f): Similarly, but for nDIC. The shaded areas are error ranges calculated from the upper and lower limits of

260 the TA (518-1006 $\mu\text{mol kg}^{-1}$) for and DIC (475-1371 $\mu\text{mol kg}^{-1}$) in ~~land water~~riverine water. The ranges are not random errors thus
have remained the same error range for monthly or yearly averaging. The dotted lines in shaded areas represent the average
values.

265 —The PLS regression showed that the explanatory variables SST, SSS, nTA, and nDIC explained well the objective
variables seawater fCO_2 ($r^2 = 0.996$) and Ω_{cal} ($r^2 = 0.997$) (Figure 5). The average contributions due to each explanatory
variable in the PLS analysis were consistent with those in the equilibrium calculation for seawater fCO_2 and Ω_{cal} using the
averages in Area B and the respective dAB values (Table S2). Area A had lower seawater fCO_2 and Ω_{cal} than Area B and
both seawater fCO_2 and Ω_{cal} showed clear seasonal variations.



Figures 5. (a): Temporal contributions in the PLS analysis by SST, SSS, nTA, and nDIC to the difference in seawater $f\text{CO}_2$ between Area A and B. (b): The corresponding monthly averages. (c): The corresponding yearly averages. (d): Temporal contributions in the PLS analysis by SST, SSS, nTA, and nDIC to the difference in Ω_{cal} between Area A and B. (e): The monthly averages. (f): The yearly averages. . The red lines represent the sum of each contribution and is almost equal to temporal variation of dAB of seawater $f\text{CO}_2$ and Ω_{cal} .

Formatted: Font: (Asian) MS 明朝, (Asian) Japanese

4. Discussion

—The extent of Area A defined using nTA (Figure 2f) was consistent with the low-salinity area of the Pacific coast of Japan (Figure 1a). The SSS south of 37°N exhibited an abrupt change in value 205.74 km from mainland Japan (Figure S4), which is consistent with the distance of the boundary between Areas A and B (246.67250 km). SSS is affected by precipitation and evaporation; therefore, nTA was a more accurate indicator of ~~landwater~~~~riverine~~ ~~water~~ than SSS. However, the consistency between the two results provides strong evidence that the nTA in Area A was derived from ~~landwater~~~~riverine~~ ~~water~~. These distances were calculated statistically using 20 years of observational data on SSS and nTA. It would be challenging to obtain a similarly significant result from single observations. Therefore, the findings of this study, which quantify the extent of the influence of ~~landwater~~~~riverine~~ ~~water~~, are novel and offer new insights.

—To evaluate the effect of the Kuroshio Current on ~~landwater~~~~riverine~~ ~~water~~ distribution, another EOF analysis was performed using data from the Kuroshio Large Meander period (2017–2020 in this study) in which the Kuroshio path followed an alternative meandering path south of its usual course (Kawabe, 1985). Area A was within the range of 353.61350 km from land, utilizing the Mode 1 EOF anomaly during the meander period, whereas it was 246.67250 km during the entire period. This result was consistent with the observed Kuroshio meandering path and supports the assumption that the Kuroshio Current ~~defines-effects~~ Area A. However, Area A extended further out of the open ocean than the Kuroshio axis during the entire study period (Figure 2f). Therefore, the Kuroshio Current limited the spread of ~~landwater~~~~riverine~~ ~~water~~ to some extent but did not completely inhibit it.

The supply of TA by ~~landwater~~~~riverine~~ ~~water~~ was higher than the time deviation of dAB for almost the entire period, suggesting that the supply was one of the main factors contributing to the increase in dAB (Figure 4). On the other hand, the annual rate of increase in the dAB of nTA was almost zero ($-0.02 \pm 0.05 \mu\text{mol kg}^{-1} \text{ year}^{-1}$). Therefore, the residual term would be the negative value of the same scale with ~~Sup_{lw}~~~~Sup_{rw}~~ term for TA. The primary cause of the negative residual term is assumed to be horizontal advection. The advection effect can be estimated from the product of the current velocity and dAB of nTA. The period of increasing dAB of nTA (Figure 3c) is consistent with the period of increasing absolute value of the residual term in Figure 4b. In addition, vertical advection could not be the main cause of the negative residual term, because the vertical gradient for calculating vertical advection was small and insignificant (see Text S1). Other causes of the residual term are differences in biological metabolism, such as calcification and nitrate consumption; calcification by coccolithophores is the most promising process for changing oceanic nTA. However, no regional difference in calcification rate of up to $10 \mu\text{mol kg}^{-1} \text{ year}^{-1}$ (Figure 4b) has not been reported between the Japanese coastal Area A (Area A) and the surrounding sea area (Area B) (Hopkins and Balch, 2018; Krumhardt et al., 2019). Another component of TA include nitrate, which is consumed during photosynthesis to raise nTA (Brewer and Goldman, 1976). The data on total nitrate (TN) concentration is available in GLODAP, and the mean values were $1.19 \pm 0.11 \mu\text{mol kg}^{-1}$ and $0.34 \pm 0.04 \mu\text{mol kg}^{-1}$ in Area A and B, respectively. As the monthly difference were largest in the winter ($2.11 \mu\text{mol kg}^{-1}$) and almost reach zero in the summer, the main source of nitrate would be vertical advection rather than input from land. Nonetheless, the effect of nitrate

on TA was probably one order of magnitude smaller than that of the ~~landwater~~riverine water supply and is negligible as the main source of nTA.

The DIC variation is more complicated than the TA variation because the spatiotemporal variation in biological metabolism and vertical advection is larger and more significant than that of TA, in addition to the effect of CO₂ exchange with the atmosphere. Unlike the TA, the seasonal variations in the ~~landwater~~riverine water supply were not consistent with those in the time derivative (Figure 4e). This trend indicated that ~~landwater~~riverine water supply was not the primary driver of DIC variation in Area A. The effect of oceanic CO₂ uptake was highly variable and unclear on a decadal scale. However, on a seasonal scale, it was more distinct, resulting in negative shifts in the summer residual terms and positive shifts in the winter residual terms. This seasonal variation indicated that the oceanic CO₂ uptake in Area A was larger than that in Area B in summer, and vice versa in winter. This was caused by the lower seawater fCO₂ in Area A during the summer season and higher wind velocity in Area B during the winter season. Consequently, the residual term of nDIC indicated a strong and complex seasonal variation, which included a maximum in the winter and two minimums in spring and summer with a difference of 100 μmol kg⁻¹ year⁻¹. Contrary to TA, DIC was affected by nutrient and organic matter loading from terrestrial sources, and was strongly affected by differences in biological metabolism between Areas A and B. For DIC, in contrast to TA, a significant vertical profile trend was observed (Text S1); consequently, some of the residual terms might have been influenced by vertical advection.

—To quantify the effect of biological metabolism, the effects of horizontal and vertical advection were estimated based on the following assumptions: 1) the residual term for nTA (C_{res_TA}) was assumed to be equal to the horizontal advection term, based on the considerations that the effects of vertical advection and biological metabolism on nTA are negligible. 2) The horizontal advection term was proportional to dAB of nTA (dAB_{TA}) and nDIC (dAB_{DIC}). Several previous studies have used normalized values for the calculation of TA and DIC advection (Broecker and Peng, 1992; Keeling and Peng, 1995) and have also proven their validity as an approximation (Robbins, 2001). Because the advection term is calculated as the product of concentration gradient and flow field, and the associated distance and flow velocity are the same at dAB_{TA} and dAB_{DIC} , it can be assumed that the horizontal advection effect on DIC (C_{hadv_DIC}) can be estimated using the following equation:

$$C_{hadv_DIC} = K \frac{dAB_{DIC}}{D_{AB}}$$

$$C_{res_TA} = K \frac{dAB_{TA}}{D_{AB}}$$

$$C_{hadv_DIC} = C_{res_TA} \cdot \frac{dAB_{DIC}}{dAB_{TA}} \quad (45)$$

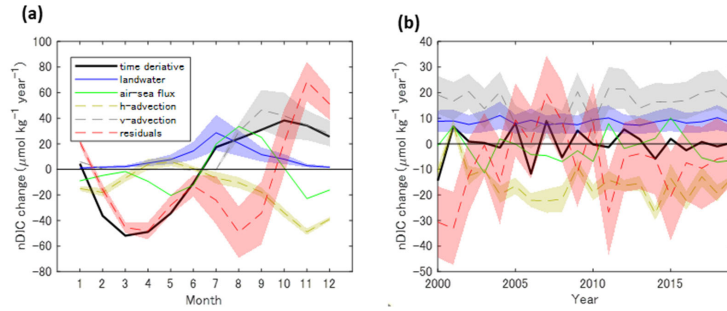
where, K and D_{AB} are the index values associated with the current field and horizontal distance between Areas A and B, respectively. These parameters were assumed to be the same for TA and DIC calculations. 3) Vertical advection for nDIC (C_{vhadv_DIC}) was estimated from mixing with subsurface water when the mixed layer was deepened. Specifically, we used a simplified equation of the method of a previous study (Ishii et al., 2001).

$$\int C_{vad} v_{DIC}(t) dt = \frac{\{\Delta nDIC(t+1) + \Delta nDIC(t)\}}{2} \times \frac{\{MLD(t+1) - MLD(t)\}}{\{MLD(t+1) \rho_{MLD(t+1)}\}}$$

$$\Delta nDIC(t) = \{nDIC(July, MLD(t)) - nDIC(t, MLD(t))\} \cdot \rho_{MLD(t)} \quad (56)$$

where, $\Delta nDIC(t)$ is the difference between the average nDIC in July ($nDIC(July)$) and the nDIC at time t at mixed layer depth ($MLD(t)$) multiplied by the seawater density at $MLD(t)$ ($\rho_{MLD(t)}$). The nDIC profile at a depth below the mixed layer was assumed to be maintained at its average value in July; as the mixed layer deepened, the difference from the July profile was added to the nDIC in the mixed layer. The effect of vertical advection on nDIC was negligible when the mixed-layer depth did not change or became shallower. The details on the calculation of the nDIC profiles are provided in Text S1.

The effects of horizontal and vertical advection on nDIC are shown in Figure 6. However, due to the large error range in the vertical advection term for each time step (the median was 137%), only the monthly and annual averages are shown in the figure. The horizontal and vertical advection effects were identified mainly from autumn to winter with an annual mean value of $-15.55 \pm 1.35 \mu\text{mol kg}^{-1} \text{ year}^{-1}$ and $15.55 \pm 2.25 \mu\text{mol kg}^{-1} \text{ year}^{-1}$, respectively (Ave \pm SE). Seasonally, the residual term had a maximum in the winter and two minimums in spring and summer, with an overall mean of $-7.30 \pm 3.24 \mu\text{mol kg}^{-1} \text{ year}^{-1}$.



Figures 6. Temporal variations of nFA-nDIC time derivative and related terms in Equation (2) (a): The monthly averages. (b): The yearly averages. The shaded areas of horizontal advection (h-advection) and vertical advection (v-advection) are the random error calculated using the error propagation (see Text S1). Therefore, unlike the error ranges of Sup_{pin} and Sup_{res} , these were reduced by $10^{-0.5}$ or $20^{-0.5}$ by monthly or yearly averaging, respectively.

Although the above results were not definitive because of many assumptions and large error ranges, the fact that the final residual term on the decadal scale was almost negative supports the idea that Area A is likely under heterotrophic conditions within the mixed layer. The positive shift in the residual term before and after 2007 was due to the low vertical advection term caused by the small MLD during winter. The 2007 minimum SST in Area A (19.41°C) was the highest of the overall annual minimum SST ($17.71 \pm 0.66^\circ\text{C}$, Ave \pm SD), and thus the surface seawater mixing would be weaker than that in other

years. Therefore, the residual term for this period does not necessarily indicate changes in biological metabolism. However, the high SST during winter suggests that the decomposition of biofixed carbon may be accelerated. Seasonally, the March-April minimum in the residual term was assumed to be the result of phytoplankton blooms in the open ocean area in Area A.

Another minimum in July-August was assumed to be due to the primary production of phytoplankton and submerged aquatic vegetation under eutrophic conditions in the inner bays and near-shore areas. The winter maximum can be explained by the upwelling of organic matter and the decomposition of bio-fixed carbons within the mixed layer.

It should be noted that the residual term above includes the effects of the water CO₂ flux in near-shore areas. However, unlike the air-sea CO₂ flux in the ocean (C_{flux} in Equation (2)), the air-water CO₂ flux in near-shore areas is very difficult to quantify because observations of water fCO₂ and the physical regulating factor defined as “transfer velocity” (e.g., Wanninkhof, 2014) are limited. The estimation of this CO₂ flux varies widely among the existing studies. For example, global average models (Aufdenkamp et al., 2011; Tranvik et al., 2009) have estimated that approximately half of the carbon supply from land is released into the atmosphere via the air-water CO₂ flux in near-shore areas. However, the inner bays affected by [landwater-riverine water](#) in this study showed a trend in atmospheric CO₂ absorption (Tokoro et al., 2021), that is unlikely to follow the global average trend. Therefore, enhanced observation and analysis of atmospheric CO₂ exchange in nearshore areas is essential for a more accurate assessment of the residual term as an indicator of biological metabolism.

—Despite Area A having a higher nDIC than Area B (Figure 3), seawater fCO₂ in Area A tended to be lower than in Area B (-3.61 ± 0.70 μ atm). This was mainly because of the lower SST and higher nTA in Area A than those in Area B (Figure 5).

The low SST can likely be attributed to [landwater-riverine water](#), which is mainly supplied by snowmelt and rainfall from the mountains and highlands and therefore tends to have lower original water temperatures. In particular, the short flow paths of Japanese rivers can likely limit the effects of heating due to solar radiation and other factors. The three inner bays with strong river influence had lower average water temperature (18.66–19.23 °C, Tokoro et al., 2021) than areas A (22.02 °C) and B (22.86 °C), which support our assumption. The decrease in seawater fCO₂ peaked in the summer (-15.90 ± 4.72 μ atm from July to September), when the decrease in nDIC due to biological metabolism and the increase in nTA due to river supply coincided. However, this decreasing in seawater fCO₂ had little effect on annual oceanic CO₂ uptake in Area A. Compared to the hypothetical case where [landwater-riverine water](#) did not affect seawater fCO₂ (seawater fCO₂ in Area A were the same as that in Area B), the change in air-sea CO₂ flux would be similar (0.00 ± 0.33 mol m⁻² year⁻¹). This was because the decrease in air-sea CO₂ flux in summer almost offsets the increase in winter. Although the increase in seawater fCO₂ in winter was smaller than the decrease in summer, the air-sea CO₂ fluxes in summer and winter were coincidentally balanced, owing to higher wind speeds in winter.

—For Ω_{cal} , seawater in Area A was notably more acidified than in the surrounding sea area, based on a 20-year average (-0.13 ± 0.01). The impact on coastal acidification was particularly significant in winter, with an average decrease of -0.25 (5.33 to 5.08). nTA was only mitigation factor for coastal acidification among the explanatory variables, and reduced acidification due to other factors to 65% (-0.20 to -0.13). This coastal acidification was found to be progressing, with dAB of

Ω_{cal} decreasing by -0.52 ± 0.14 per decade. This can be attributed to an increasing trend in dAB of nDIC ($0.32 \pm 0.08 \mu\text{mol kg}^{-1} \text{year}^{-1}$) due to the trend of increasing precipitation in Japan.

5. Conclusions

In this study, we identified areas affected by landwater/riverine water in the Northwest Pacific Ocean by using statistically processed observational data. We also evaluated the contribution of landwater/riverine water to oceanic CO_2 uptake and coastal acidification by comparing the TA and DIC values in the sea area affected by landwater/riverine water and surrounding sea areas.

The Area A affected by landwater/riverine water (Area A) was within 246.67250 km of mainland Japan and, to some extent, along the Kuroshio axis. This area was consistent with the low-SSS area ~~of low-SSS~~ on the Pacific coast of Japan. In addition, the range increased to 353.64350 km during the period when the Kuroshio Current meandered south, indicating that the Kuroshio Current path influences the spread of landwater/riverine water.

Both nTA and nDIC were higher in surrounding sea ~~in-of~~ Area A. The main source of TA was landwater/riverine water in summer, which was balanced by a decrease due to horizontal advection in autumn and winter. The DIC flows were more complex than the TA flows and were more strongly affected by a residual term than by the landwater/riverine water supply. The contribution of biological metabolism is expected to be more influential on the residual term after excluding the horizontal and vertical advection effects. Biological metabolism showed a maximum in winter and two minima in spring and summer. The annual mean suggests heterotrophic conditions within the mixed layer in Area A. In any case, because the air-water CO_2 flux in near-shore areas is still difficult to estimate, a more thorough quantification of DIC flow in relation to landwater/riverine water needs to be considered.

—Seawater fCO_2 in Area A decreased mainly in summer because of the supplied landwater/riverine water, which has low-temperature water with high nTA. However, landwater/riverine water supply was found to have virtually no effect on oceanic CO_2 uptake at an annual scale. This is because CO_2 emission was enhanced by strong wind speeds in winter, in addition to the relatively small increase in seawater fCO_2 in winter. The change in the air-sea CO_2 flux in winter was coincidentally balanced by the change in summer, and the annual average was almost zero. Although acidification progressed more in Area A than in the surrounding sea area, the supply of TA by landwater/riverine water mitigated the acidification to 65%. However, an increase in precipitation may have led to increases in nDIC and acidification in Area A.

—This study makes a significant contribution to the analysis of carbon flows in the boundary seawater between terrestrial and oceanic areas because the quantification of carbon flows in these areas is often uncertain in space and time. Enhancing the observational data allows the results to be spatially extended to larger regional or global scales. The analysis results are expected to have a smaller error range owing to the high spatiotemporal resolution of the vertical profiles of the carbonate data and air-water CO_2 flux data in near-shore areas.

Data Availability

435 The SSS, SST, and fCO₂ in air and seawater datasets are available in the SOCAT database (Pfeil et al., 2013; Bakker et al.,
2016, <https://socat.info/index.php/data-access/>). The TA and DIC data were available from the GLODAP database version
2.2020 (Key et al., 2015; Olsen et al., 2016; Olsen, 2020, <https://glodap.info/>). Wind speed data were obtained from the
CCMP database (version 2.0) (Atlas et al., 2011; Mears et al., 2019; <https://data.remss.com/ccmp/v02.0/>). The river flow
440 datasets were obtained from the Water Information System of the Ministry of Land, Infrastructure, Transport, and Tourism of
Japan (<http://www1.river.go.jp/>). Vertical water temperature datasets for calculating MLD were obtained from the JCOPE2M
dataset (Miyazawa et al., 2017, 2019, . <https://www.jamstec.go.jp/jcope/htdocs/distribution/>).

Author Contribution

TT designed the study and wrote the first draft on the manuscript. SN, ST, SS, SD, KE, MI, NK, TO, KT, and YN supplied
445 and managed data for SOCAT and GLODAP. SN supported data processing. All authors contributed to manuscript writing
and proofing.

Competing interests

The contact author has declared that none of the authors have any competing interests.

450

Acknowledgments

We appreciate the cooperation of Toyofuji Shipping Co. and Kagoshima Senpaku Co. in the NIES VOS program. We also
thank the captains and crews of M/S Pyxis, M/S New Century 2, M/S Trans Future 5, R/V Mirai, R/V Hakuho-maru, R/V
Keifu-maru, R/V Ryofu-maru, R/V Wakataka-maru, and R/V Soyo-maru. This research was financially supported by the
455 Global Environmental Research Coordination System, Ministry of the Environment, Japan (grant numbers MOE1751 and
MOE 2252) and CREST, Japan Science and Technology Agency (grant number JPMJCR23J4).

References

Andreev, A. G. and Pavlova, G. Y.: Marginal Seas, in: Carbon and nutrient fluxes in continental margins, edited
460 by Liu, K. K., Atkinson, L., Quiñones, R., and Talaue-McManus, L., Springer, New York, 395–406, 2009.

Atlas, R., Hoffman, R. N., Ardizzone, J., Leidner, S. M., Jusem, J. C., Smith, D. K., and Gombos, D.: A Cross-calibrated Multiplatform Ocean Surface Wind Velocity Product for Meteorological and Oceanographic Applications, *Bull. Amer. Meteor. Soc.*, 92, 157–174. <https://doi.org/10.1175/2010BAMS2946.1>, 2011.

465

Aufdenkampe, A. K., Mayorga, E., Raymond, P. A., Melack, J. M., Doney, S. C., Alin, S. R., Aalto, R. E., and Yoo, K.: Riverine coupling of biogeochemical cycles between land, oceans, and atmosphere, *Front. Ecol. Environ.*, 9, 53–60. <https://doi.org/10.1890/100014>, 2011.

470 Bakker, D. C. E., Pfeil, B., Landa, C. S., Metzl, N., O'Brien, K. M., Olsen, A., Smith, K., Cosca, C., Harasawa, S., Jones, S. D., Nakaoka, S., Nojiri, Y., Schuster, U., Steinhoff, T., Sweeney, C., Takahashi, T., Tilbrook, B., Wada, C., Wanninkhof, R., Alin, S. R., Balestrini, C. F., Barbero, L., Bates, N. R., Bianchi, A. A., Bonou, F., Boutin, J., Bozec, Y., Burger, E. F., Cai, W. J., Castle, R. D., Chen, L., Chierici, M., Currie, K., Evans, W., Featherstone, C., Feely, R. A., Fransson, A., Goyet, C., Greenwood, N., Gregor, L., Hankin, S., Hardman-

475 Mountford, N. J., Harlay, J., Hauck, J., Hoppema, M., Humphreys, M. P., Hunt, C. W., Huss, B., Ibáñez, J. S. P., Johannessen, T., Keeling, R., Kitidis, V., Körtzinger, A., Kozyr, A., Krasakopoulou, E., Kuwata, A., Landschützer, P., Lauvset, S. K., Lefèvre, N., Lo Monaco, C., Manke, A., Mathis, J. T., Merlivat, L., Millero, F. J., Monteiro, P. M. S., Munro, D. R., Murata, A., Newberger, T., Omar, A. M., Ono, T., Paterson, K., Pearce, D., Pierrot, D., Robbins, L. L., Saito, S., Salisbury, J., Schlitzer, R., Schneider, B., Schweitzer, R., Sieger, R.,
480 Skjelvan, I., Sullivan, K. F., Sutherland, S. C., Sutton, A. J., Tadokoro, K., Telszewski, M., Tuma, M., van Heuven, S. M. A. C., Vandemark, D., Ward, B., Watson, A. J., and Xu, S.: A multi-decade record of high-quality fCO₂ data in version 3 of the Surface Ocean CO₂ Atlas (SOCAT), *Earth Syst. Sci. Data*, 8, 383–413. <https://doi.org/10.5194/essd-8-383-2016>, 2016.

485 Bauer, J. E., Cai, W. J., Raymond, P. A., Bianchi, T. S., Hopkinson, C. S., and Regnier, P. A. G.: The changing carbon cycle of the coastal ocean, *Nature*, 504, 61–70. <https://doi.org/10.1038/nature12857>, 2013.

Borges, A. V., Delille, B., and Frankignoulle, M.: Budgeting sinks and sources of CO₂ in the coastal ocean: Diversity of ecosystems counts, *Geophys. Res. Lett.*, 32, L14601. <https://doi.org/10.1029/2005GL023053>, 2005.

490

Brewer, P. G. and Goldman, J. C.: Alkalinity changes generated by phytoplankton growth, *Limnol. Oceanogr.*, 21, 108–117. <https://doi.org/10.4319/lo.1976.21.1.0108>, 1976.

- Broecker, W. S. and Peng, T. H.: Tracers in the sea, Eldigio Press, New York, 1982.
- 495 Broecker, W. S. and Peng, T. H.: Interhemispheric transport of carbon dioxide by ocean circulation, *Nature*, 356, 587–589. <https://doi.org/10.1038/356587a0>, 1992.
- Cai, W. J.: Estuarine and coastal ocean carbon paradox: CO₂ sinks or sites of terrestrial carbon incineration? *Ann. Rev. Mar. Sci.*, 3, 123–145. <https://doi.org/10.1146/annurev-marine-120709-142723>, 2011.
- 500 Carstensen, J. and Duarte, C. M.: Drivers of pH variability in coastal ecosystems, *Environ. Sci. Technol.*, 53, 4020–4029. <https://doi.org/10.1021/acs.est.8b03655>, 2019.
- 505 Chen, C. T. A. and Borges, A. V.: Reconciling opposing views on carbon cycling in the coastal ocean: Continental shelves as sinks and near-shore ecosystems as sources of atmospheric CO₂, *Deep Sea Research Part II: Topical Studies in Oceanography*, 56, 578–590. <https://doi.org/10.1016/j.dsr2.2009.01.001>, 2009.
- Chen, C. T. A., Huang, T. H., Chen, Y. C., Bai, Y., He, X., and Kang, Y.: Air-sea exchanges of CO₂ in the world’s coastal seas, *Biogeosciences*, 10, 6509–6544. <https://doi.org/10.5194/bg-10-6509-2013>, 2013.
- 510 de Boyer Montégut, C., Madec, G., Fischer, A. S., Lazar, A., and Iudicone, D.: Mixed layer depth over the global ocean: An examination of profile data and a profile-based climatology, *J. Geophys. Res.*, 109. <https://doi.org/10.1029/2004JC002378>, 2004.
- 515 Denbo, D. W. and Allen, J. S.: Rotary empirical orthogonal function analysis of currents near the Oregon Coast, *J. Phys. Oceanogr.*, 14, 35–46. [https://doi.org/10.1175/1520-0485\(1984\)014<0035:REOFAO>2.0.CO;2](https://doi.org/10.1175/1520-0485(1984)014<0035:REOFAO>2.0.CO;2), 1984.
- Duarte, C. M., Hendriks, I. E., Moore, T. S., Olsen, Y. S., Steckbauer, A., Ramajo, L., Carstensen, J., Trotter, J. A., and McCulloch, M.: Is ocean acidification an open-ocean syndrome? Understanding anthropogenic impacts on seawater pH, *Estuaries Coasts*, 36, 221–236. <https://doi.org/10.1007/s12237-013-9594-3>, 2013.
- 520

- Fitzer, S. C., Torres Gabarda, S. T., Daly, L., Hughes, B., Dove, M., O'Connor, W., Potts, J., Scanes, P., and Byrne, M.: Coastal acidification impacts on shell mineral structure of bivalve mollusks, *Ecol. Evol.*, 8, 8973–8984. <https://doi.org/10.1002/ecc3.4416>, 2018.
- Friis, K., Körtzinger, A., and Wallace, D. W. R.: The salinity normalization of marine inorganic carbon chemistry data, *Geophys. Res. Lett.*, 30. <https://doi.org/10.1029/2002GL015898>, 2003.
- Holte, J. and Talley, L.: A new algorithm for finding mixed layer depths with applications to argo data and Subantarctic mode water formation, *J. Atmos. Ocean. Technol.*, 26, 1920–1939. <https://doi.org/10.1175/2009JTECHO543.1>, 2009.
- Hopkins, J. and Balch, W. M.: A new approach to estimating coccolithophore calcification rates from space, *JGR Biogeosciences.*, 123, 1447–1459. <https://doi.org/10.1002/2017JG004235>, 2018.
- Inoue, H. Y., Matsueda, H., Ishii, M., Fushimi, K., Hirota, M., Asanuma, I., and Takasugi, Y.: Long-term trend of the partial-pressure of carbon-dioxide ($p\text{CO}_2$) in surface waters of the western North Pacific, 1984–1993, *Tellus B.*, 47, 391–413. <https://doi.org/10.1034/j.1600-0889.47.issue4.2.x>, 1995.
- Ishii, M., Inoue, H. Y., Matsueda, H., Saito, S., Fushimi, K., Nemoto, K., Yano, T., Nagai, H., and Midorikawa, T.: Seasonal variation in total inorganic carbon and its controlling processes in surface waters of the western North Pacific subtropical gyre, *Mar. Chem.*, 75, 17–32. [https://doi.org/10.1016/S0304-4203\(01\)00023-8](https://doi.org/10.1016/S0304-4203(01)00023-8), 2001.
- Kawabe, M.: Sea level variations at the Izu Islands and typical stable paths of the Kuroshio, *J. Ocean. Soc. Jpn*, 41, 307–326. <https://doi.org/10.1007/BF02109238>, 1985.
- Keeling, R. and Peng, T. H.: Transport of heat, CO_2 , and O_2 by the Atlantic's thermohaline circulation, *Phil. Trans. R. Soc. Lond. B*, 348, 133–142. <https://doi.org/10.1098/rstb.1995.0055>, 1995.
- Kessouri, F., McWilliams, J. C., Bianchi, D., Sutula, M., Renault, L., Deutsch, C., Feely, R. A., McLaughlin, K., Ho, M., Howard, E. M., Bednaršek, N., Damien, P., Molemaker, J., and Weisberg, S. B.: Coastal eutrophication

drives acidification, oxygen loss, and ecosystem change in a major oceanic upwelling system, Proc. Natl Acad. Sci. U. S. A., 118. <https://doi.org/10.1073/pnas.2018856118>, 2021.

555

Key, R. M., Olsen, A., van Heuven, S., Lauvset, S. K., Velo, A., Lin, X., Schirnick, C., Kozyr, A., Tanhua, T., Hoppema, M., Jutterström, S., Steinfeldt, R., Jeansson, E., Ishii, M., Perez, F. F., and Suzuki, T.: Global ocean data analysis project, version 2, (GLODAPv2), Oak Ridge National Laboratory/CDIAC-162, NDP-093, Carbon Dioxide Information Analysis Center, Oak Ridge National Laboratory, United States Department of Energy, Oak Ridge, TN. https://doi.org/10.3334/CDIAC/OTG_NDP093_GLODAPv2. [dataset] 2015.

560

Killick, R., Fearnhead, P., and Eckley, I. A.: Optimal detection of changepoints with a linear computational cost, J. Am. Stat. Assoc., 107, 1590–1598. <https://doi.org/10.1080/01621459.2012.737745>, 2012.

565

Kitamura, T., Nakano, T., and Sugimoto, S.: Decadal variations in mixed layer salinity in the Kuroshio Extension recirculation gyre region: Influence of precipitation during the warm season, J. Oceanogr., 72, 167–175. <https://doi.org/10.1007/s10872-015-0317-1>, 2016.

Krumhardt, K. M., Lovenduski, N. S., Long, M. C., Levy, M., Lindsay, K., Moore, J. K., and Nissen, C.:

570

Coccolithophore growth and calcification in an acidified ocean: Insights from community earth system model simulations, J. Adv. Model. Earth Syst., 11, 1418–1437. <https://doi.org/10.1029/2018MS001483>, 2019.

Lee, K., Tong, L. T., Millero, F. J., Sabine, C. L., Dickson, A. G., Goyet, C., Park, G. H., Wanninkhof, R., Feely, R. A., and Key, R. M.: Global relationships of total alkalinity with salinity and temperature in surface waters of the world's oceans, Geophys. Res. Lett., 33. <https://doi.org/10.1029/2006GL027207>, 2006.

575

Lehmann, N., Lantuit, H., Böttcher, M. E., Hartmann, J., Eulenburg, A., and Thomas, H.: Alkalinity generation from carbonate weathering in a silicate-dominated headwater catchment at Iskorasfjellet, northern Norway, Biogeosciences, 20, 3459–3479. <https://doi.org/10.5194/bg-20-3459-2023>, 2023.

580

Lewes, E., and Wallace, D. W. R.: Program Developed for CO₂ System Calculations, ORNL/CDIAC-105, Carbon Dioxide Information Analysis Center, Oak Ridge National Laboratory, U.S. Department of Energy, Oak Ridge, TN, USA, <https://doi.org/10.15485/1464255>, 1998.

Formatted: Subscript

585 Mears, C. A., Scott, J., Wentz, F. J., Ricciardulli, L., Leidner, S. M., Hoffman, R., and Atlas, R.: A near-real-time
version of the Cross-Calibrated Multiplatform (CCMP) ocean surface wind velocity data set, JGR Oceans, 124,
6997–7010. <https://doi.org/10.1029/2019JC015367> [dataset], 2019.

590 Millero, F. J., Lee, K., and Roche, M.: Distribution of alkalinity in the surface waters of the major oceans, Mar.
Chem., 60, 111–130. [https://doi.org/10.1016/S0304-4203\(97\)00084-4](https://doi.org/10.1016/S0304-4203(97)00084-4), 1998.

Miyama, T., Minobe, S., and Goto, H.: Marine heatwave of sea surface temperature of the Oyashio region in
summer in 2010–2016, Front. Mar. Sci., 7. <https://doi.org/10.3389/fmars.2020.576240>, 2021.

595 Miyazawa, Y., Kuwano-Yoshida, A., Doi, T., Nishikawa, H., Narazaki, T., Fukuoka, T., and Sato, K.:
Temperature profiling measurements by sea turtles improve ocean state estimation in the Kuroshio-Oyashio
Confluence region, Ocean Dyn., 69, 267–282. <https://doi.org/10.1007/s10236-018-1238-5> [dataset], 2019.

600 Miyazawa, Y., Varlamov, S. M., Miyama, T., Guo, X. Y., Hihara, T., Kiyomatsu, K., Kachi, M., Kurihara, Y.,
and Murakami, H.: Assimilation of high-resolution sea surface temperature data into an operational
nowcast/forecast system around Japan using a multi-scale three-dimensional variational scheme, Ocean Dyn., 67,
713–728. <https://doi.org/10.1007/s10236-017-1056-1> [dataset], 2017.

605 Mucci, A.: The solubility of calcite and aragonite in seawater at various salinities, temperatures, and one
atmospheric pressure, Am. J. Sci., 283, 780-799, <https://doi.org/10.2475/ajs.283.7.780>, 1983.

610 Murata, A. M., Kaneko, I., Nemoto, K., Fushimi, K., and Hirota, M.: Spatial and temporal variations of surface
seawater $f(\text{CO}_2)$ in the Kuroshio off Japan, Mar. Chem., 59, 189–200. [https://doi.org/10.1016/S0304-4203\(97\)00096-0](https://doi.org/10.1016/S0304-4203(97)00096-0), 1998.

Olsen, A., Key, R. M., van Heuven, S., Lauvset, S. K., Velo, A., Lin, X. H., Schirnack, C., Kozyr, A., Tanhua, T.,
Hoppema, M., Jutterström, S., Steinfeldt, R., Jeansson, E., Ishii, M., Pérez, F. F., and Suzuki, T.: The Global
Ocean Data Analysis Project version 2 (GLODAPv2) - An internally consistent data product for the world ocean,
Earth Syst. Sci. Data, 8, 297–323. <https://doi.org/10.5194/essd-8-297-2016> [dataset], 2016.

Formatted: Font: (Asian) MS 明朝, (Asian) Japanese

Formatted: Default Paragraph Font, Font: 10 pt

Formatted: Font: (Asian) MS 明朝, (Asian) Japanese

615

Olsen, A., Lange, N., Key, R. M., Tanhua, T., Bittig, H. C., Kozyr, A., Álvarez, M., Azetsu-Scott, K., Becker, S., Brown, P. J., Carter, B. R., Cotrim da Cunha, L., Feely, R. A., van Heuven, S., Hoppema, M., Ishii, M., Jeansson, E., Jutterström, S., Landa, C. S., Lauvset, S. K., Michaelis, P., Murata, A., Pérez, F. F., Pfeil, B., Schirnack, C., Steinfeldt, R., Suzuki, T., Tilbrook, B., Velo, A., Wanninkhof, R., and Woosley, R. J.: An updated version of the global interior ocean biogeochemical data product, GLODAPv2.2020., *Earth Syst. Sci. Data*, 12, 3653–3678. <https://doi.org/10.5194/essd-12-3653-2020>, 2020.

620

Passow, U. and Carlson, C. A.: The biological pump in a high CO₂ world, *Mar. Ecol. Prog. Ser.*, 470, 249–271. <https://doi.org/10.3354/meps09985>, 2012.

625

Pfeil, B., Olsen, A., Bakker, D. C. E., Hankin, S., Koyuk, H., Kozyr, A., Malczyk, J., Manke, A., Metzl, N., Sabine, C. L., Akl, J., Alin, S. R., Bates, N., Bellerby, R. G. J., Borges, A., Boutin, J., Brown, P. J., Cai, W. J., Chavez, F. P., Chen, A., Cosca, C., Fassbender, A. J., Feely, R. A., González-Dávila, M., Goyet, C., Hales, B., Hardman-Mountford, N., Heinze, C., Hood, M., Hoppema, M., Hunt, C. W., Hydes, D., Ishii, M., Johannessen, T., Jones, S. D., Key, R. M., Körtzinger, A., Landschützer, P., Lauvset, S. K., Lefèvre, N., Lenton, A., Laurantou, A., Merlivat, L., Midorikawa, T., Mintrop, L., Miyazaki, C., Murata, A., Nakadate, A., Nakano, Y., Nakaoka, S., Nojiri, Y., Omar, A. M., Padin, X. A., Park, G. H., Paterson, K., Perez, F. F., Pierrot, D., Poisson, A., Ríos, A. F., Santana-Casiano, J. M., Salisbury, J., Sarma, V. V. S. S., Schlitzer, R., Schneider, B., Schuster, U., Sieger, R., Skjelvan, I., Steinhoff, T., Suzuki, T., Takahashi, T., Tedesco, K., Telszewski, M., Thomas, H., Tilbrook, B., Tjiputra, J., Vandemark, D., Veness, T., Wanninkhof, R., Watson, A. J., Weiss, R., Wong, C. S., and Yoshikawa-Inoue, H.: A uniform, quality controlled Surface Ocean CO₂ Atlas (SOCAT), *Earth Syst. Sci. Data*, 5, 125–143. <https://doi.org/10.5194/essd-5-125-2013>, 2013.

630

635

Rassmann, J., Lansard, B., Pozzato, L., and Rabouille, C.: Carbonate chemistry in sediment porewaters of the Rhône River delta driven by early diagenesis (northwestern Mediterranean), *Biogeosciences*, 13, 5379–5394. <https://doi.org/10.5194/bg-13-5379-2016>, 2016.

640

Regnier, P., Friedlingstein, P., Ciais, P., Mackenzie, F. T., Gruber, N., Janssens, I. A., Laruelle, G. G., Lauerwald, R., Luysaert, S., Andersson, A. J., Arndt, S., Arnosti, C., Borges, A. V., Dale, A. W., Gallego-Sala, A., Goddérís, Y., Goossens, N., Hartmann, J., Heinze, C., Ilyina, T., Joos, F., LaRowe, D. E., Leifeld, J., Meysman,

645

F. J. R., Munhoven, G., Raymond, P. A., Spahni, R., Suntharalingam, P., and Thullner, M.: Anthropogenic perturbation of the carbon fluxes from land to ocean, *Nature Geosci.*, 6, 597–607.
<https://doi.org/10.1038/Ngeo1830>, 2013.

650 Regnier, P., Resplandy, L., Najjar, R. G., and Ciais, P.: The land-to-ocean loops of the global carbon cycle, *Nature*, 603, 401–410. <https://doi.org/10.1038/s41586-021-04339-9>, 2022.

Robbins, P. E.: Oceanic carbon transport carried by freshwater divergence: Are salinity normalizations useful? *J. Geophys. Res.*, 106, 30939–30946. <https://doi.org/10.1029/2000JC000451>, 2001.

655

Romero-Mujalli, G., Hartmann, J., and Börker, J.: Temperature and CO₂ dependency of global carbonate weathering fluxes – Implications for future carbonate weathering research, *Chem. Geol.*,
<https://doi.org/10.1016/j.chemgeo.2018.08.010>, 2018.

Formatted: Subscript

Formatted: Default Paragraph Font, Font: 10 pt

Formatted: Font: (Asian) MS 明朝, (Asian) Japanese

660 Sugimoto, S., Takahashi, N., and Hanawa, K.: Marked freshening of North Pacific subtropical mode water in 2009 and 2010: Influence of freshwater supply in the 2008 warm season, *Geophys. Res. Lett.*, 40, 3102–3105.
<https://doi.org/10.1002/grl.50600>, 2013.

Taguchi, F., Fujiwara, T., Yamada, Y., Fujita, K., and Sugiyama, M.: Alkalinity in coastal seas around Japan, *Bull. Coast. Oceanogr.*, 47, 71–75, 2009.

665

Takahashi, T., Sutherland, S. C., Sweeney, C., Poisson, A., Metzl, N., Tilbrook, B., Bates, N., Wanninkhof, R., Feely, R. A., Sabine, C., Olafsson, J., and Nojiri, Y.: Global sea-air CO₂ flux based on climatological surface ocean pCO₂, and seasonal biological and temperature effects, *Deep Sea Research Part II: Topical Studies in Oceanography*, 49, 1601–1622. [https://doi.org/10.1016/S0967-0645\(02\)00003-6](https://doi.org/10.1016/S0967-0645(02)00003-6), 2002.

670

Takahashi, T., Sutherland, S. C., Wanninkhof, R., Sweeney, C., Feely, R. A., Chipman, D. W., Hales, B., Friederich, G., Chavez, F., Sabine, C., Watson, A., Bakker, D. C. E., Schuster, U., Metzl, N., Yoshikawa-Inoue, H., Ishii, M., Midorikawa, T., Nojiri, Y., Körtzinger, A., Steinhoff, T., Hoppema, M., Olafsson, J., Arnarson, T. S., Tilbrook, B., Johannessen, T., Olsen, A., Bellerby, R., Wong, C. S., Delille, B., Bates, N. R., and de Baar, H. J. W.: Climatological mean and decadal change in surface ocean pCO₂, and net sea-air CO₂ flux over the global

675

oceans, *Deep Sea Research Part II: Topical Studies in Oceanography*, 56, 554–577.

<https://doi.org/10.1016/j.dsr2.2008.12.009>, 2009.

680 Takamura, T. R., Inoue, H. Y., Midorikawa, T., Ishii, M., and Nojiri, Y.: Seasonal and interannual variations in
pCO₂(sea) and air-sea CO₂ fluxes in midlatitudes of the western and eastern North Pacific during 1999–2006:
Recent results utilizing voluntary observation ships, *J. Meteorol. Soc. Jpn*, 88, 883–898.
<https://doi.org/10.2151/jmsj.2010-602>, 2010.

685 Takatani, Y., Enyo, K., Iida, Y., Kojima, A., Nakano, T., Sasano, D., Kosugi, N., Midorikawa, T., Suzuki, T., and
Ishii, M.: Relationships between total alkalinity in surface water and sea surface dynamic height in the Pacific
Ocean, *J. Geophys. Res. Oceans*, 119, 2806–2814. <https://doi.org/10.1002/2013JC009739>, 2014.

Tokoro, T., Nakaoka, S., Takao, S., Kuwae, T., Kubo, A., Endo, T., and Nojiri, Y.: Contribution of biological
690 effects to carbonate-system variations and the air-water CO₂ flux in urbanized bays in Japan, *JGR Oceans*, 126.
<https://doi.org/10.1029/2020JC016974>, 2021.

Tokoro, T., Nakaoka, S., Takao, S., Saito, S., Sasano, D., Enyo, K., Ishii, M., Kosugi, N., and Nojiri, Y.:
Statistical analysis of spatiotemporal variations of air-sea CO₂ fluxes in the Kuroshio region, *JGR Oceans*, 128.
695 <https://doi.org/10.1029/2023JC019762>, 2023.

Tranvik, L. J., Downing, J. A., Cotner, J. B., Loiselle, S. A., Striegl, R. G., Ballatore, T. J., Dillon, P., Finlay, K.,
Fortino, K., Knoll, L. B., Kortelainen, P. L., Kutser, T., Larsen, S., Laurion, I., Leech, D. M., McCallister, S. L.,
McKnight, D. M., Melack, J. M., Overholt, E., Porter, J. A., Prairie, Y., Renwick, W. H., Roland, F., Sherman, B.
700 S., Schindler, D. W., Sobek, S., Tremblay, A., Vanni, M. J., Verschoor, A. M., von Wachenfeldt, E., and
Weyhenmeyer, G. A.: Lakes and reservoirs as regulators of carbon cycling and climate, *Limnol. Oceanogr.*, 54,
2298–2314. https://doi.org/10.4319/lo.2009.54.6_part_2.2298, 2009.

Wallace, R. B., Baumann, H., Gear, J. S., Aller, R. C., and Gobler, C. J.: Coastal Ocean acidification: The other
705 eutrophication problem, *Estuarine Coast. Shelf Sci.*, 148, 1–13. <https://doi.org/10.1016/j.ecss.2014.05.027>, 2014.

Wanninkhof, R.: Relationship between wind speed and gas exchange over the ocean revisited, Limnol. Oceanogr. Methods, 12, 351–362. <https://doi.org/10.4319/lom.2014.12.351>, 2014.

710 Weiss, R. E.: Carbon dioxide in water and seawater: The solubility of a non-ideal gas, Mar. Chem., 2(3), 203–
215. [https://doi.org/10.1016/0304-4203\(74\)90015-2](https://doi.org/10.1016/0304-4203(74)90015-2), 1974.

▲
Wold, S., Sjöström, M., and Eriksson, L.: PLS-regression: A basic tool of chemometrics, Chemom. Intell. Lab. Syst., 58, 109–130. [https://doi.org/10.1016/S0169-7439\(01\)00155-1](https://doi.org/10.1016/S0169-7439(01)00155-1), 2001.

715 Yoshikawa-Inoue, H., Midorikawa, T., and Takamura, T. R.: Temporal and spatial variations in carbonate system and air-sea CO₂ flux in the Kuroshio and Kuroshio Extension, in: Western Pacific air-sea interaction study, edited by Uematsu, M., Yokouchi, Y., Watanabe, Y. W., Takebe, S., and Yamanaka, Y., Terra Publishing, Tokyo, 2014. <https://doi.org/10.5047/w-pass.a02.004>.

720 Zeebe, R. E. and Wolf-Gladrow, D.: CO₂ in seawater: Equilibrium, kinetics and isotopes, Elsevier Science, Amsterdam, 2001.

Formatted: Font: Not Italic
Formatted: Font: Not Italic
Formatted: Font: Not Bold
Formatted: Default Paragraph Font, Font: 10 pt, Not Bold
Formatted: Font: (Asian) MS 明朝, (Asian) Japanese